High-performance, multi-channel, fiber-based absolute distance measuring interferometer system

Leslie L. Deck

Zygo Corporation, Laurel Brook Road, Middlefield, CT. USA, 06455-0448

ABSTRACT

I describe the principle of operation and performance of a fiber-based absolute distance measuring interferometer system with 60 independent simultaneous channels. The system was designed for demanding applications requiring passive, electrically immune sensors with an extremely long MTTF. In addition to providing better than 0.3nm measurement repeatability at 5KHz for all channels, the system demonstrated absolute distance uncertainty of less than 5nm over a 500 micron measurement range.

1. INTRODUCTION

Today's advanced manufacturing systems often need to monitor and control dozens, and even hundreds, of degrees of freedom simultaneously. Examples of these systems can be found in the semiconductor, mass storage, automotive and medical equipment industries. Each degree of freedom can represent a different physical property, requiring different sensors to evaluate. Incorporating independent commercial sensors to accomplish this task is costly and complicates the overall system interface architecture since one has to deal with a variety of different I/O schemes. As a consequence, data acquisition and synchronization becomes very difficult.

This paper describes a heterodyne-based absolute distance measuring interferometry (ADMI) system* designed to address demanding applications requiring a large number of independent channels. The system is fiber based for flexibility and uses telecom wavelengths and components for high reliability.[1 2] Each simultaneously sampled channel has a 500micron measurement range with a bandwidth of 5KHz. In addition, each channel can measure the absolute distance with an uncertainty of less than 5nm over the full measurement range with a measurement bandwidth of better than 50Hz. Though primarily designed for motion measurement, the sensors can be easily configured for measuring a wide variety of physical properties. The channels are immune to electromagnetic interference, completely passive and deposit less than 50microwatts of optical energy into the monitored system.

In this paper I describe the ADMI system, the methods used for calculating and correcting the interferometric signals, some of the calibration and error compensation strategies and methods used to verify performance.

2. MEASUREMENT PRINCIPLES

2.1. Relative measurements

The measurement principle is based on a heterodyned interferometric coupled cavity, shown in Figure 1 along with descriptions of the intermediate fields. Broad-band illumination is input from the left with optical frequency ω and mean wavenumber k and split into two paths in a first cavity, called the heterodyne cavity. The two paths in the heterodyne cavity have different optical path lengths L_1 and L_2, and one leg (L_1) linearly modulates the optical path with a phase angular velocity v. The two beams recombine and enter the test cavity whose two legs have optical path lengths L_3 and L_4 and recombine again to produce the output intensity shown. The output consists of a DC term, a homodyne term which depends only on changes in the test cavity optical path difference (OPD), and three terms that oscillate at the

* The techniques and systems described in this paper are protected by U.S. and foreign patents or patents pending.

heterodyne frequency. Of the three heterodyne terms, one is proportional to changes in the heterodyne cavity OPD and the other two are proportional to the difference in the OPDs between the two cavities.

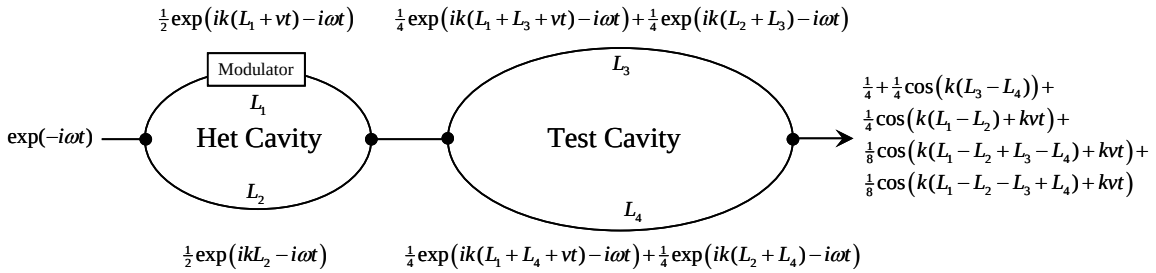

Figure 1: Coupled cavity interferometer with intermediate field descriptions. The output intensity is described on the right.

If the illumination is broad-band with coherence length Γ, inspection of the output intensity terms in Figure 1 verifies that high contrast interference from the test cavity at the heterodyne frequency only occurs if $|L_1 - L_2| >> \Gamma$ and $|L_1 - L_2| - |L_3 - L_4| < \Gamma$. Though this geometry seems complex, it has a number of very convenient and useful qualities;

1. The use of broad-band illumination eliminates coherent noise
2. Heterodyning can be performed remotely from the sensing
3. Test and reference beams identified via OPD (rather than another attribute like polarization)
4. Working distance is decoupled from measurement range

Some of these qualities will be made clearer in the system description section.

2.2. Absolute distance measurements

In order to provide an electronic "home" capability for each channel, the absolute cavity length is measured. The absolute length measurement principle must be rapid, precise and compatible with the relative measurement architecture to minimize the cost per function. The method chosen is multi-wavelength interferometry (MWI) using the method of exact fractions. In this method the fringe order is obtained through the successive application of "equivalent wavelengths" of decreasing length. The equivalent wavelengths are actually the wavelengths of the interference beat between two base wavelengths via;

$$\lambda_{eq} = \lambda_1 \lambda_2 / |\lambda_1 - \lambda_2|. \quad (1)$$

Choosing appropriate base wavelengths can produce equivalent wavelengths of any desired length. The number of wavelengths to use depends on the measurement range and the phase measurement uncertainty. For the measurement range considered for this system, three base wavelengths compatible with the illumination source were employed.

3. SYSTEM DESCRIPTION

The ADMI system can be conveniently separated into 5 subsystems or modules shown in Figure 2; an illumination module, a heterodyne module, a distribution module, a detection/analysis module and the sensing subsystem. In a typical measurement, the three wavelengths are first sequentially cycled through and their phases measured to derive the absolute distance for each channel. Afterwards, the system uses a single wavelength to monitor relative changes to that absolute distance. A description of each subsystem follows.

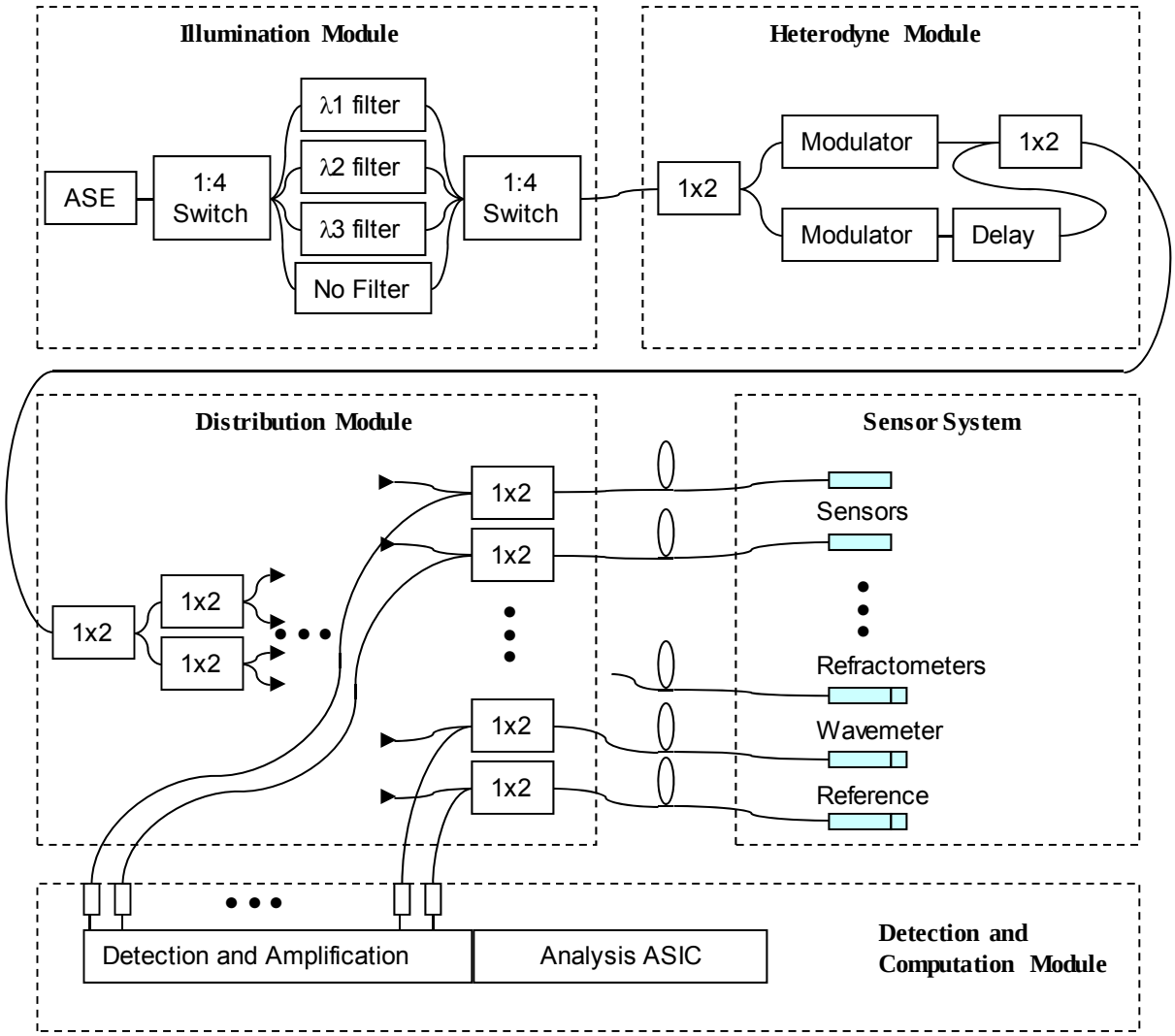

Figure 2: Block diagram of the ADMI system showing major components.

3.1. Illumination Module (IM)

The IM must provide the correct spectral width and intensity at each of the three base wavelengths and rapidly switch between them. For this purpose, a broadband amplified spontaneous emission (ASE) source is used to cover the required spectral band and custom transmission filters extract the spectral shape at the 3 base wavelengths. MEMS switches select the appropriate wavelength with switching times of less than 4msec. One of the switch options includes sending the raw ASE output through an amplitude modulator. This option is used for various in-situ calibrations.

Working within the ASE spectral bandwidth, we selected 1530nm, 1530.75nm and 1560nm for the 3 base wavelengths, producing equivalent wavelengths of 80 microns and 2mm. This selection represents a good compromise between light efficiency and absolute measurement performance.

The spectral shape produced by the filters is important since the width defines the coherence length and the shape influences the location of observable interference and the phase linearity. Ideally, the spectral shape produces a single coherence peak that smoothly falls to zero on either side. A Gaussian shaped spectrum provides just this feature and so the filters were designed to follow this shape with a FWHM of about 3nm; Figure 3 shows the measured transmission shape from one of the filters compared to an ideal Gaussian.

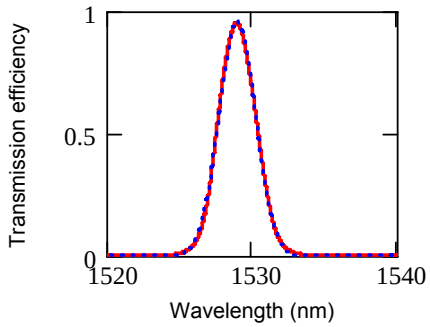

Figure 3: The measured spectral shape of a filter (red lines) compared to a perfect Gaussian (blue dots).

3.2. Heterodyne Module (HM)

The HM accepts the wavelength selected by the IM and sends it through an unbalanced Mach-Zehnder (MZ) interferometer cavity where at least one leg is phase-shift modulated. In practice the MZ is constructed with a modulator in both legs to minimize differences in thermal sensitivity. One modulator operates with serrodyne modulation[3] to produce the primary high-speed phase shifting. In serrodyning, the optical path is modulated with a linear sawtooth, adjusted to deviate the phase by 2π radians, so that all but one of the first sidebands are suppressed. The electro-optic modulator has a bandwidth of 500MHz, minimizing the flyback time. Distortions in the serrodyne signal (and the flyback) contribute to small cyclic phase errors that are post-corrected with proprietary algorithms.† The HM cavity OPD is factory set to equal the nominal OPD of the sensors used. Note that though the illumination coherence length determines the measurement range, the HM cavity OPD sets the sensor working distance. Thus the working distance is decoupled from the measurement range; an important property for many applications.

3.3. Distribution Module (DM)

The DM is a fully common path, passive module that successively splits the light with a 6 layer pyramidal cascade of 1x2 splitters into 64 independent channels. A seventh layer of 1x2 splitters provide the way to both transmit the light and receive the return signal from the sensors. The return signal is then routed to the detection and computation module.

3.4. Sensor subsystem

The sensor subsystem consists of a variety of sensors designed to monitor position, wavelength, refractive index and heterodyne cavity drift. With small differences, all the sensors are variations of a Fizeau interferometer geometry and consist of a fiber whose end face has a thermally expanded core (TEC) separated from a Gradient Index (GRIN) lens by a specific gap (Figure 4). The beam waist is set to a fixed working distance from the end of the GRIN, whose last surface acts as the cavity reference surface. These basic sensors are small, stable and inexpensive.

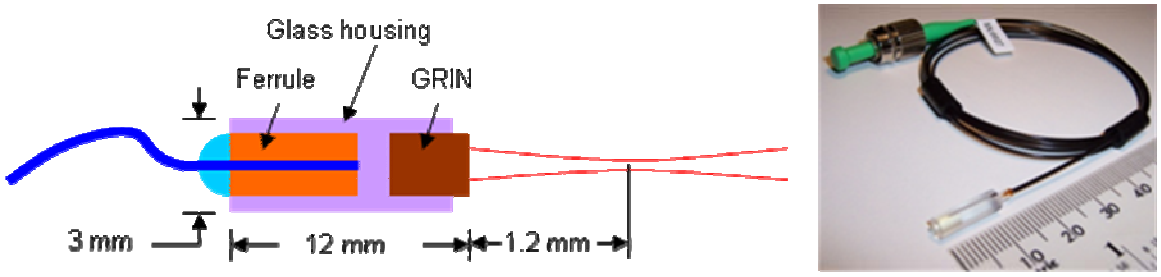

Figure 4: Basic sensor design. The last surface of the GRIN lens is used as the reference surface.

This basic design is used for position sensing by situating a reflecting test surface at the beam waist position. The returning signal is the interference between the wavefronts reflected from the GRIN reference surface and the test surface.

---

† For example, U.S. Patent Nos. 7,428,685 and 6,950,192 to Zygo

Variants to the basic design produce specialized sensors. The reference sensor, used to monitor the heterodyne cavity drift, measures the interference from a fixed cavity made from optically contacted plates. In this case the last surface of the GRIN is angled and AR coated so as not to interfere with the reference cavity measurement. The wavemeter sensor is made identically to the reference sensor but with a different cavity OPD. The refractometer sensor is also made identically to the reference sensor, but with the cavity open to the air.

3.5. Detection and Computation Module (DCM)

The DCM converts the light returning from the test cavity to an amplified electrical signal and then filters and digitizes the signal for processing at a bandwidth of 1 MHz. Since the serrodyne modulation nominally produces a pure sinusoidal intensity modulation, the phase is extracted with a sliding window discrete Fourier transform (DFT). The basic analysis flow for one channel is shown in Figure 5 and the process occurs in each channel in parallel.

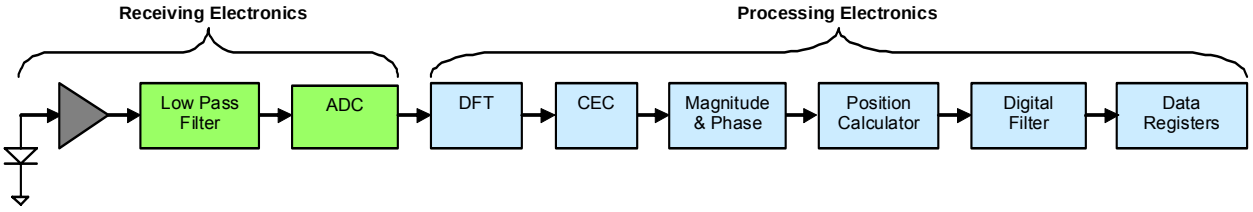

Figure 5: Channel amplification, digitization and phase computation flow.

The CEC block stands for Cyclic Error Correction which removes nonlinear errors produced by imperfections in the serrodyne modulation. The signal magnitude and phase is then extracted from the complex DFT amplitude.

The position calculator block next computes the physical distances from the computed phases. Consider the analysis for a single relative position measurement at the start of the process where the absolute positions/phases are unknown. The computation assumes that the absolute phase Φ is related to the physical distance via

$$\Phi = 2\pi D/\lambda + \alpha\,, \tag{2}$$

where D is the total OPD and λ the mean illumination wavelength. The α represents the sum of all system phase offsets (such as phase change on reflection and electronic phase offsets). We further assume that α is a slow function of time. Invariably, environmental and aging affects will create drifts in wavelength and refractive index, so the system must also be able to measure these quantities. The process starts by measuring the wavelength. The CORDIC block produces a modulo-2π phase ϕ for the reference and wavemeter channels;

$$\tilde{\phi}_R = \mathrm{mod}_{2\pi}\left(2\pi\tilde{D}_R/\lambda + \alpha_R\right), \quad \tilde{\phi}_W = \mathrm{mod}_{2\pi}\left(2\pi\tilde{D}_R/\lambda + \alpha_W\right), \tag{3}$$

where the subscripts R and W represent reference and wavemeter channels respectively. I use the tilde (~) to represent measured quantities and lower case symbols for modulo-2π phases. The OPDs $\tilde{D}_W$, $\tilde{D}_R$ are absolutely known premeasured quantities. Using Eqs. (4), the wavemeter channel's phase is subtracted from the reference channel to eliminate heterodyne cavity variations and the mean wavelength is measured via;

$$\tilde{\lambda} = \frac{2\pi\left(\tilde{D}_W - \tilde{D}_R\right)}{\tilde{\phi}_W - \tilde{\phi}_R - \tilde{\Delta}_{WR}}\,, \tag{4}$$

where $\tilde{\Delta}_{WR} = \alpha_W - \alpha_R$ is the measured phase offset between those two channels. Note that the starting wavelength must be known well enough to distinguish between 2π uncertainties in the phase difference $\tilde{\phi}_W - \tilde{\phi}_R$. This is accomplished by premeasuring the filter spectra, providing a mean wavelength starting uncertainty of less than 100pm. If a refractometer is employed, the phase equation for that channel is;

$$\tilde{\phi}_N = \mathrm{mod}_{2\pi}\left(2\pi\tilde{D}_N/\lambda + \alpha_N\right) = \mathrm{mod}_{2\pi}\left(4\pi n\tilde{G}_N/\lambda + \alpha_N\right), \tag{5}$$

where $\tilde{D}_N$ is replaced with $2n\tilde{G}_N$ with n and $\tilde{G}_N$ the index and measured refractometer cavity gap respectively. Subtracting the reference channel and using the measured wavelength and phase offset one gets;

$$\tilde{n} = \frac{\frac{\tilde{\lambda}}{2\pi}\left(\tilde{\phi}_N - \tilde{\phi}_R - \tilde{\Delta}_{NR}\right) + \tilde{D}_R}{2\tilde{G}_N}. \tag{6}$$

Note that the when the refractometer gap $\tilde{G}_N$ is calibrated, one must either measure or estimate the refractive index. We use Edlens equation[4] for this purpose while monitoring pressure, humidity and temperature. Finally, the physical gap in the test channel $\tilde{G}_T$ is found assuming the phase equation;

$$\tilde{\phi}_T = \mathrm{mod}_{2\pi}\left(2\pi\tilde{D}_T/\lambda + \alpha_T\right) = \mathrm{mod}_{2\pi}\left(4\pi n\tilde{G}_T/\lambda + \alpha_T\right). \tag{7}$$

Subtracting the reference channel and using the measured wavelength, index and phase offset one gets;

$$\tilde{G}_T = \frac{\frac{\tilde{\lambda}}{2\pi}\left(\tilde{\phi}_T - \tilde{\phi}_R - \tilde{\Delta}_{TR}\right) + \tilde{D}_R}{2\tilde{n}}. \tag{8}$$

All of these computations occur in the Position Calculator block. Note that running values of the mean wavelength and index are available throughout the measurement. The final positions are output to the user through data registers that are updated at 5KHz and can be arbitrarily polled.

4. METROLOGY CONSIDERATIONS AND CALIBRATIONS

I briefly discuss here some of the more important factors that needed consideration to provide the best metrology performance.

4.1. Gaussian Beams

The sensor beam follows Gaussian beam propagation, so the beam divergence half-angle is $\Theta_{1/2} = w_0/z_R$ where w_0 is the $1/e^2$ beam waist radius and $z_R = \pi w_0^{\,2}/\lambda$ is the characteristic Rayleigh range. The sensor is designed to have a beam waist radius of about 50microns, so beam divergence is non-negligible. The effect of this divergence on the phase evolution is compensated for once the absolute OPD, beam waist position and Rayleigh range are known.

4.2. Electronic phase offsets and data delay

Electronic component tolerances and channel dependent fiber lengths mean that each channel will experience a slightly different phase offset during amplification, which will propagate through the analysis. As seen in Eqs. 3-5, these phase offsets are all relative to the reference channel. The method of exact fractions is particularly sensitive to these offsets, so they must be measured and accounted for. The offsets and delays are measured with proprietary algorithms using the unfiltered ASE spectrum.

4.3. Spectrum asymmetries

Asymmetries in the base wavelength spectra can produce nonlinearities in the cavity phase versus OPD relationships. To account for this the spectra are premeasured. As with the corrections for divergence, this correction is applied once the absolute OPD is measured.

4.4. Monitor absolute OPD calibrations

The absolute OPD of the various monitors (reference, wavelength and refractometer) must be known and this calibration is done in two steps. First a broadly tunable source using Fourier transform interferometry[5] to compare the interferometric phase evolution from the monitor against a known cavity measures the OPD to within 10nm. Subsequently, angle tuning interferometry[6] is used to refine this to ~1nm.

5. SYSTEM PERFORMANCE

The performance of the two measurement modes; high-speed relative measurements using a single wavelength, and absolute distance measurements using the 3-wavelength algorithm, were assessed differently.

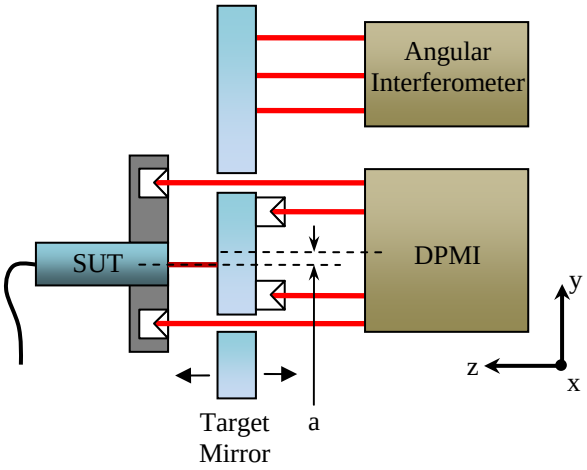

Figure 6: Setup used to compare the ADMI relative and absolute measurement modes against simultaneous measurements of a ZMI-4000 for a 500um scan centered about the beam waist.

5.1. Relative measurement performance

To assess ADMI relative mode performance, distance measurements were taken while the cavity was mechanically scanned over the full measurement range and compared with simultaneous measurements from a collinear commercial HeNe based distance measuring interferometer system (Zygo ZMI-4000) with a differential plane mirror interferometer (DPMI). The layout of the experiment is shown in Figure 6. Both piston and tilt motion of the target mirror was obtained and the tilt information was used to correct for additional z motion from the Abbé offset “a”.

When in relative measurement mode, where the cavity phase variation is measured using a single wavelength, the two measurements agreed with the ZMI-4000 to within 1nm rms (Figure 7). The residual indicates a small difference about the center remains, which is most likely due to an imperfect spectrum correction. Multiple measurements agree within 1nm.

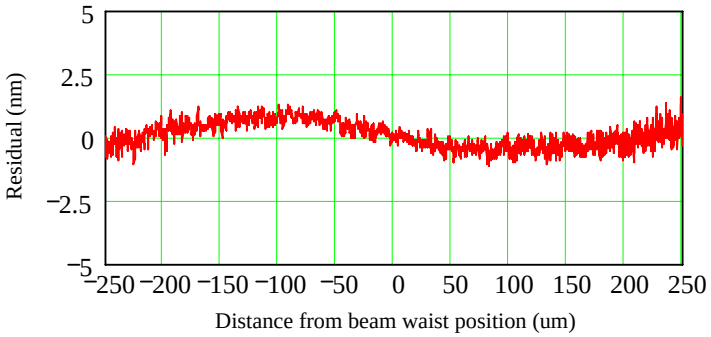

Figure 7: Difference between the ADMI system and simultaneous measurements with a ZMI-4000 for a 500um scan centered about the beam waist.

5.2. Absolute measurement performance

Unfortunately, the ZMI-4000 only provides relative displacements and thus cannot be used to corroborate the absolute measurements directly. Thus the fidelity of the absolute measurement mode was determined via a two step process;

1) Measure an absolutely known cavity within the measurement range
2) Compare a sequence of absolute measurements during a scan across the measurement range against simultaneous measurements with the ZMI-4000

The first step verifies the absolute uncertainty of the system at one point within the measurement range, while the second verifies that performance across the full measurement range.

In the first step, the ADMI measured a fixed cavity that had been absolutely calibrated using the methods described previously. The cavity had a physical gap of 1009.8996 microns. The cavity was measured approximately every 15 minutes over a period of 72 hours and Figure 8 shows the measured deviation from the nominal “known” value. The figure shows that the absolute measurements agree with the calibrated value to within 3nm peak-valley.

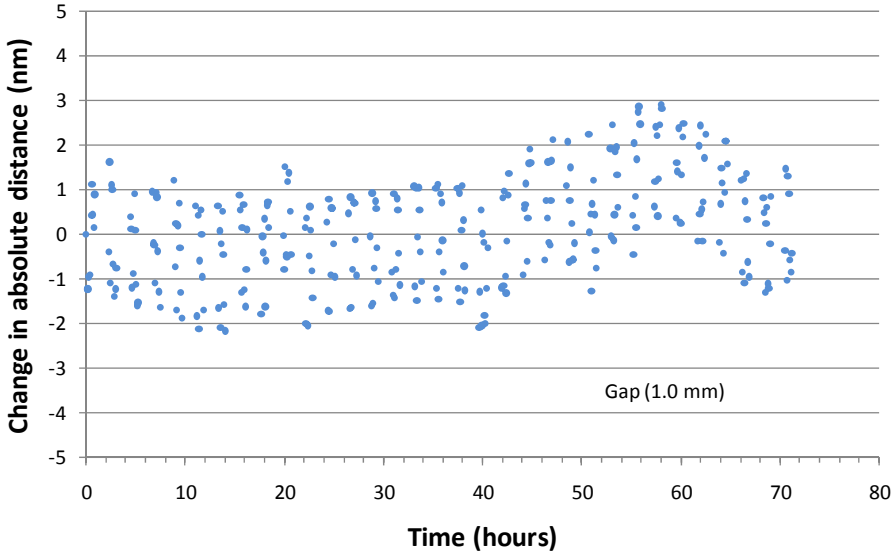

Figure 8: A plot of 300 measurements over 72 hours of the absolutely known cavity using the ADMI.

In the second step, the ADMI measured the cavity gap continuously using the three-wavelength absolute mode while the cavity gap was scanned in a manner identical to that used to measure the performance of the relative measurement mode. In this situation the absolute gap is imperfectly known, however since the previous step has demonstrated that the ADMI correctly measured the gap at the position indicated, we can infer that the full range was correctly measured.

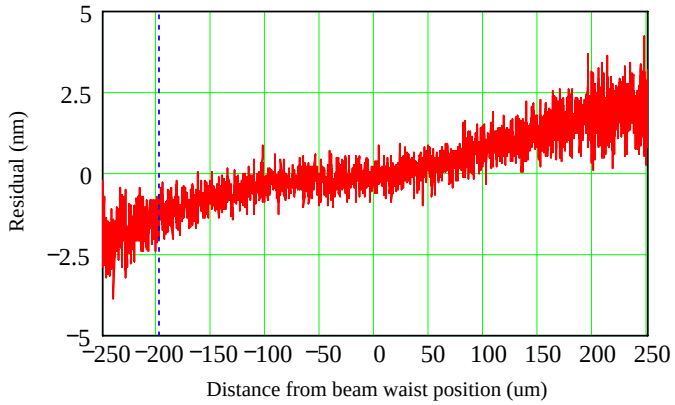

Figure 9: Difference between the ADMI system in absolute measurement mode and simultaneous measurements with a ZMI-4000 for a 500um scan centered about the beam waist. A constant 302.5nm overall piston error was subtracted from the measurements, which just represented the difference in the zero position between the ADMI and the ZMI-4000. The vertical dotted blue line represents the position of the fixed cavity measured previously.

6. SUMMARY

The construction and performance of a fiber-based absolute distance measuring interferometer system with >60 independent simultaneous channels was described. Each channel has a pre-defined working distance and is capable of independently and simultaneously measuring absolute distance over a 500 micron range. The sensors are rugged, passive, electrically immune and deposit very little energy into the test environment. All channels have a measurement repeatability of 0.3nm at 5KHz and an absolute distance uncertainty of less than 5nm over the full 500 micron measurement range.

ACKNOWLEDGEMENTS

A system of this complexity is the product of a very capable and innovative team. It is a pleasure to recognize the many contributions from Vivek Badami, Robert Carangelo, Frank Demarest, Colin Fletcher, Gregg Gallatin, Kurt Redlitz and Lars Selberg to this work.

REFERENCES

[1] O. Jusko et. al., “Form measurement by optical and tactile scanning,” Proc. SPIE 7133, 71333A (2009)
[2] V. Badami, T. Blalock, “Uncertainty evaluation of a fiber-based interferometer for the measurement of absolute dimensions,” Proc. SPIE 5879, 587903 (2005)
[3] M. Laroche et. al., “Serrodyne optical frequency shifting for heterodyne self-mixing in a distributed-feedback fiber laser,” Opt. Lett. 33 (23), 2746-2748 (2008)
[4] N. Bobroff, “Recent advances in displacement measuring interferometry,” in "Measurement Science and technology,” V4, No 9 (1993)
[5] L. Deck, “Fourier-Transform Phase Shifting Interferometry,” Appl. Opt. 42(13), 2354-2365 (2003)
[6] V. Badami, L. Deck, L. Selberg, “Measurement of the absolute distance between two partially reflective surfaces,” Proc. ASPE 2761, 144-147 (2008)